CONF-950445--2

STATIC FLOW INSTABILITY IN SUBCOOLED FLOW BOILING IN PARALLEL CHANNELS*

Moshe Siman-Tov
Dave K. Felde
Joel L. McDuffee
Graydon L. Yoder, Jr.
Engineering Technology Division
Oak Ridge National Laboratory
P.O. Box 2009
Oak Ridge, Tennessee 37831-8218

For presentation at the
2nd Internationl Conference on Multiphase Flow
April 3-7, 1995
Kyoto, Japan

*Research sponsored by the Office of Energy Research, U.S. Department of Energy, under contract DE-AC05-84OR21400 with Martin Marietta Energy Systems, Inc.

GH

STATIC FLOW INSTABILITY IN SUBCOOLED FLOW BOILING IN PARALLEL CHANNELS

Moshe Siman-Tov
Dave K. Felde
Joel L. McDuffee
Graydon L. Yoder, Jr.

Engineering Technology Division
Oak Ridge National Laboratory*
Oak Ridge, Tennessee

ABSTRACT

A series of tests for static flow instability or flow excursion (FE) at conditions applicable to the proposed Advanced Neutron Source reactor was completed in parallel rectangular channels configuration with light water flowing vertically upward at very high velocities. True critical heat flux experiments under similar conditions were also conducted. The FE data reported in this study considerably extend the velocity range of data presently available worldwide. Out of the three correlations compared, the Saha and Zuber correlation had the best fit with the data. However, a modification was necessary to take into account the demonstrated dependence of the Stanton *(St)* and Nusselt *(Nu)* numbers on subcooling levels, especially in the low subcooling regime.

INTRODUCTION

The Advanced Neutron Source (ANS) is a state-of-the-art research facility proposed for construction on the U.S. Department of Energy's Oak Ridge Reservation. ANS will be the world's most advanced facility for neutron

---

*Managed by Martin Marietta Energy Systems, Inc., under contract DE-AC05-84OR21400 with the U.S. Department of Energy.

beam experiments. To meet the requirements, the core of the ANS reactor (ANSR) must be designed to accommodate very high power densities using a very large coolant mass flux and a high level of subcooling. A statistical/probabilistic uncertainty analysis is being performed to determine safety margins and optimal power [1].

Because of its multiparallel channels configuration, the ANSR core is subject to FE and/or flow instability [2] that may occur once boiling is initiated in any one of the channels. The FE phenomenon, also referred to as the onset of flow instability (OFI), constitutes a different thermal limit from a true critical heat flux (CHF) or departure from nucleate boiling (DNB). In a system subject to FE, initiation of boiling in one of the channels can result in flow redistribution to the other cooler channels. This process can rapidly lead to flow starvation in the hot channel, leading in turn to a local CHF or DNB at a flow lower than the nominal flow rate. After incipient boiling (IB) starts, the pressure gradient rises very gradually until the onset of net vapor generation (ONVG) point or the point of onset of significant void (OSV), where both void generation and pressure gradient start increasing sharply. Because of the sharp acceleration in void generation occurring after OSV, it is normally accepted that FE or OFI will likely occur soon after OSV is established.

The available correlations and experimental data bases for FE and CHF seldom include the specific combination of ANSR operating parameters (see the data comparison and correlation section below). Maulbetsch and Griffith [3] and other investigators have demonstrated that excursive instability will occur in a channel if

$$\frac{d(\Delta P_{sup})}{dQ} > \frac{d(\Delta P_{dem})}{dQ} \quad . \qquad (1)$$

In the case of many parallel channels between large common headers, as in the ANSR, the slope of the external supply system is practically zero (constant pressure drop). Based on this observation, FE or OFI conditions were determined in most of the experiments of this study by detecting the minimum in pressure-drop on the demand curve as the flow was reduced in steps under a constant heat flux. This method allowed for repetition of many nondestructive FE tests without experiencing an actual FE that normally causes test section failure.

In most cases, FE will precede true CHF in a parallel channel configuration, such as the ANSR [4]. It is noteworthy, however, that the margin between FE and CHF narrows as the level of certain parameters increases, and, at a certain point, the trend may even be reversed [5]. Since the ANSR will normally operate at moderate pressures and very high mass flux and subcooling levels, one of the main goals of these tests is to determine the relationship between CHF and FE under ANSR conditions.

EXPERIMENTAL DESIGN AND PROCEDURES

The thermal-hydraulic test loop (THTL) was designed and built to allow experimental determination of the FE and CHF thermal limits under anticipated ANS thermal-hydraulic (T/H) conditions [6]. The test section simulates a single subchannel in the ANSR core with a cross-section (Fig. 1) that has full prototypic length (507 mm), the same flow-channel gap (1.27 mm), and the same material (Al-6061). The channel span was scaled down to 12.7 mm (vs 87 and 70 mm for the upper and lower elements in the ANSR core) to limit the total power requirements to the test section. To simplify the experimental design and operation, the involute shape of the plates was not simulated. The test section wall thickness on the flat sections was 2.54 mm (vs 1.27 mm fuel plate thickness in the ANSR), as dictated by the voltage/current characteristics of the available power supplies. Reduced wall thickness at the curved ends was designed to lower the heat flux and prevent premature burnout in this area of the channel. The test channel thermocouples were placed on the back of both sides of the channel for redundancy (Fig. 1).

Most of the FE tests (without burnout) were conducted in a stiff mode, where constant flow is maintained in the channel. Other FE tests were performed in a soft system, where a constant pressure drop is maintained, resulting in actual FE and subsequent burnout. To be able to operate the system in these modes, special design features were incorporated [6, 7]. An experimental data reduction model was developed for single-phase forced-convection flow, focusing on the flat portion of the test channel. Uncertainties were estimated by the root-sum-square method, including most of the measured and data reduction components with the values (at the two standard deviation level) for the major parameters being $Lb = 4\%$, $P = 5.8\%$, $T_b = 2.0\%$, $\Delta T_{sub} =$

3.0%, Q = 3.4%, G = 5.4%, q''_{cr} = 6.4%, and St = 12.4%. A description of the data reduction program, as well as a discussion of various uncertainties in testing implementation, are provided by Siman-Tov et al. [8].

RESULTS AND DISCUSSION

The current THTL experimentation for the ANSR T/H correlations emphasizes the FE phenomenon and, to a lesser extent, CHF. The initial phase of this activity was reported by Siman-Tov et al. [8]. Since then, additional experiments have covered higher heat fluxes and velocities. The experiments completed so far include the following nominal T/H conditions:

- light water coolant,
- rectangular channel: 1.27 × 12.7 × 507 mm (Fig. 1) and 1.27 × 25.4 × 507 mm,
- inlet coolant temperature: 45 and 400C,
- exit coolant pressure: 1.7, 0.45, and 0.17 MPa,
- exit heat flux range: 0.7-18 MW/m^2, and
- corresponding exit velocity range: 2.8 28.4 m/s.

Acquiring FE data at these heat fluxes and velocities is significant for two reasons. First, to our knowledge, few data are available for FE at velocities higher than 10 m/s (the few exceptions are Waters [4], Maulbetsch and Griffith [3], and Croft [9]) and none are known above 18 m/s. The range of data has now been extended to a velocity of 28.4 m/s (at the exit), which is above the maximum velocity expected in the ANSR, including uncertainties. Second, the high heat flux achieved in this study (16.8 MW/m^2 average and 17.9 MW/m^2 at the exit) is well above the ANSR nominal average heat flux of 5.9 MW/m^2 and nominal peak heat flux of 12 MW/m^2. In fact, it is almost as high as the ANSR local hot channel peaking factor heat flux (e.g., peak heat flux with uncertainties) of 18 MW/m^2.

A summary of the pertinent data from all of the tests (FE and CHF) is given in Table 1. The St numbers for the nondestructive THTL data are plotted against subcooling in Fig. 2 (see further discussion later). The actual local heat fluxes near the exit where the FE phenomena typically occur are indicated in Table 1 as q''_{cr}. These heat flux values at the exit are higher than the average as a result of the temperature dependence of the aluminum electrical resistivity.

In addition to the nondestructive FE experiments, a number of destructive (actual burnout) tests were performed using a soft system to determine the effect of bypass ratio on FE conditions. Three such destructive FE tests were performed and the results are presented in Fig. 3. The FE318B test was designed to provide benchmark FE data under conditions similar to those under which the Costa [10] data were obtained. The minimum pressure-drop point was achieved at a velocity of 4.7 m/s compared with 5.4 m/s found by Costa, which is a reasonable agreement.

Tests FE212A and FE331A allowed investigation of the effect of bypass ratio on the actual FE burnout in relation to the minimum point in each. Both tests are for a nominal average heat flux of 12 MW/m^2, but FE212A had a bypass ratio of 2.6 while that of FE331A was 6.2 the highest bypass possible for the loop at that velocity. The minimum pressure-drop points were achieved at 19.3 and 19.5 m/s, respectively, showing the anticipated close agreement. However, the actual destructive FE failures came at velocities of 17.8 m/s for the FE212A test (bypass ratio of 2.6) and 18.4 m/s for the FE331A test (bypass ratio of 6.2), both at lower velocities than the corresponding minimum points. This comparison is consistent with expectations that higher bypass ratios should cause the actual FE to approach closer to the minimum point. The minimum pressure-drop technique for determining FE conditions is clearly a conservative estimate since it implies an ideally constant pressure drop boundary condition, as would be the case for an infinite bypass.

Two CHF experiments, CF115B and CF328A, were performed in a stiff system with a closed bypass line, by further reducing the velocity after the minimum pressure-drop point was achieved. Both experiments were conducted under similar conditions with average heat fluxes of 10.5 and 11.8 MW/m^2, respectively. The results are presented in Fig. 3 with the rest of the burnout cases. The occurrence of CHF was clearly identified in the experiments by a rapid burnout and failure of the test channel. In none of these tests was a true CHF (or the subsequent expected burnout) encountered before reaching the minimum point at which FE usually occurs. The CHF showed a 30% additional margin in velocity (14.5 m/s) compared with the FE velocity of 19.8 m/s corresponding to the minimum pressure-drop point. This margin between FE and CHF was surprisingly large based on the values predicted by the respective correlations.

Two FE tests, FE620B and CF622B, and a CHF test, CF622B, were performed with double the normal channel span (25.4 mm vs 12.7 mm) in order to determine span scalability to the 70 87 mm wide channels in the ANSR. The primary goal was to investigate any possible end effects from the channel corners, where the heat flux was reduced to 36% of that at the flat portion. Nonuniform spanwise fluid bulk temperature, spanwise fluid mixing (or the lack of it), and spanwise heat redistribution in the aluminum walls could all be dependent on span size and correspondingly affect the test results. As can be seen in Table 1 and Fig. 2, the results of the two wider span tests seem to have somewhat higher *St* numbers but are not inconsistent with the general data collected to date. Other researchers have demonstrated that there is little spanwise fluid mixing in such rectangular channels even under two-phase flow conditions [4, 10]. Furthermore, some data show that span width (or span to gap ratio) has no significant effect on either CHF or FE [11, 12]. Nevertheless, additional tests are planned to verify this conclusion.

DATA COMPARISON AND CORRELATION

The collected THTL data were compared with correlations by Costa [10], Whittle and Forgan (W&F) [11], and Saha and Zuber (S&Z) [13] in a common formulation as discussed by Siman-Tov et al. [7, 8]. All three correlations seem to be generally conservative compared with the data with the S&Z correlation having the closest fit. The Costa correlation compares reasonably well with the THTL data in the low-velocity range (below 10 m/s) but becomes increasingly conservative as velocity increases.

The above data comparison supported a shift from the Costa correlation to the S&Z correlation for the ANSR, especially since the nominal conditions of most of the accident scenarios analyzed in the ANSR involve rather high mass fluxes. Although a reasonable selection based on direct data comparison, the W&F correlation was not selected because of its global rather than local nature. This characteristic of the W&F correlation becomes a major liability for nonuniform heat flux distributions, which exist both axially and spanwise in the ANSR and when statistical uncertainties are applied in the analysis.

The S&Z correlation seems to be a good selection for the ANSR conditions because it represents the data quite well

over the entire range of interest. However, the limiting heat flux based on the original S&Z correlation is very sensitive to the subcooling value at low subcooling and decreases to zero as subcooling reaches zero. This is obviously unrealistic since the FE heat flux cannot be lower than the IB heat flux. Therefore, it became useful to plot both the THTL data and the rest of the ANS data base for FE and OSV in terms of the *St* and *Nu* numbers (which are the selected dimensionless group in the original S&Z correlation) against subcooling as shown in Figs. 4 and 5, respectively. The initial version of this data base was presented by Siman-Tov et al. [1, 14]. The data base was further expanded to include additional data at the low *Pe* number range. The current data base includes 802 data points from 33 sources (including 31 THTL data points) as summarized in Table 2.

As can be seen in both Figs. 3 and 4, there is a clear trend for the *St* number to increase with declining subcooling, particularly at lower subcoolings. A similar trend can be detected for *Nu* number in Fig. 5 but the trend is obviously not as consistent. In addition, it should be observed that by definition both the *St* and *Nu* numbers must become infinite when the subcooling is zero, which contradicts the constant values for these parameters suggested by the original S&Z correlation. This observation, in combination with the trend observed in the data, provides a strong case for modifying the S&Z constant *St* number (0.0065) and constant *Nu* number (455) criteria, especially in the low subcooling range. A best fit was developed based on the 505 data points of the data base presented by Siman-Tov et al. [14], including 26 data points from THTL. Under guidelines and constraints listed in Siman-Tov et al. [14], the following subcooling correction factor was employed to improve the original S&Z correlations for the ANS applications:

$$St = q''/(G\, C_p\, \Delta T_{sub}) = 0.0065\ \eta_{sub}\,, \qquad Pe > 70{,}000; \quad (2)$$

$$Nu = q''\, D_h / (k\, \Delta T_{sub}) = 455\ \eta_{sub}\,, \qquad Pe < 70{,}000; \quad (3)$$

where $\eta_{sub} = 0.55 + 11.21/\Delta T_{sub}$ (η_{sub} being the proposed subcooling correction factor). Figures 4 and 5 show the selected modified correlations in terms of *St* number and *Nu* number, respectively, against the expanded ANS data base

(802 data points, including 31 from THTL tests). Table 3 provides the statistics for the modified S&Z correlation in terms of mean and standard deviation, as well as for the original S&Z and Costa correlations for the same data base.

The following comments should be noted concerning the proposed modification.

(1) As seen in Table 3, the modified S&Z correlation provides considerable improvement in the uncertainties compared with either the original S&Z correlation (especially at low subcooling) or the Costa correlation (especially at high velocities). The mean and standard deviation in *St* number were 1.07 and 22%, respectively, when comparing the THTL data with the original S&Z correlation, and 1.03 and 16% when comparing them with the modification. Comparison with the worldwide data base showed a mean and standard deviation of 1.4 and 52%, respectively, for the original S&Z correlation and 1.02 and 30% for the modification.

(2) The original S&Z correlation (using *St* and *Nu* numbers) for predicting OSV were modified based on a mixture of actual FE and OSV data. Therefore, the modified correlations here are probably more reflective of FE than of OSV.

(3) There is a definite advantage for the ANSR analysis to treat the statistical uncertainties in at least two velocity zones: a low velocity ($V < 8$ m/s) and a high velocity zone ($V > 8$ m/s). The correlation uncertainties for the second zone, which includes the ANSR nominal and early transient conditions, are considerably lower than those of the first.

(4) Fitting the correlation factor with the data was constrained to be common to both *St* and *Nu* numbers. Emphasis was put on achieving a better fit with the *St* number, resulting in a compromise for the *Nu* number.

(5) The large uncertainties currently shown for the *Nu* number nodilization are obviously impractical for application to very low safety margins. It is therefore necessary in those cases to conservatively use the incipient boiling criteria (or the more conservative but simpler criterion of $T_w = T_{sat}$) as the lowest limit for all FE predictions.

(6) The uncertainties shown in Table 3 are based on the data base currently available (Table 2). With additional analytical work, further screening of the data, and additional in-house experimental efforts, the proposed modification can

be improved and the uncertainties reduced, especially those for the *Nu* number.

SUMMARY AND CONCLUSIONS

1. A modification for predicting the S&Z correlation FE was proposed to account the trend of increased *St* and *Nu* numbers with reduced subcooling and also to be consistent with the definition of these two parameters. The proposed modification provides better agreement and smaller standard deviations than either the Costa or the original S&Z correlation, based on both the THTL data and the broader ANS data base.

2. Acquiring FE data at this level of heat flux and velocity is highly significant. Most of the available FE data are in the low velocity range (< 10 m/s) and none are available above 18 m/s. The data reported in this paper extend this data range up to 28.4 m/s, well beyond the ANSR nominal velocity of 25 m/s.

3. A true CHF (or the subsequent expected burnout) was not encountered before the minimum pressure drop (FE) point in any of the experiments performed thus far. Furthermore, the two true CHF tests performed at a nominal 12 MW/m^2 showed a 5 m/s (close to 30%) reduction in limiting velocity compared with the corresponding FE tests.

4. The results of the two wider span tests performed show results with a somewhat higher *St* number. However, they are not inconsistent with the rest of the data. Additional tests are planned to confirm this conclusion.

5. Although a modification to the S&Z correlation was proposed for FE prediction, final correlation of the data for FE and CHF will be postponed until additional experiments and data analyses are performed.

ACKNOWLEDGMENTS

The authors would like to acknowledge the support of the ANS Project Office that made this work possible and the help received from George Farquharson, Lara James, Marshall McFee, Yogi Murayama, Bill Nelson, Art Ruggles, and other contributors.

NOTATION

b = flow channel gap (m)

C_p = mean coolant specific heat (kJ/kg•K)
D_h = heated diameter (m)
G = mass flux (kg/m^2•s)
k = thermal conductivity (kW/m•K)
Nu = Nusselt number $= \frac{q''D_h}{k\Delta T_{sub}}$
P = pressure (Pa)
Pe = Peclet number $= \frac{N}{St} = \frac{GC_pD_h}{k}$
Q = flow rate (m^3/s)
q'' = heat flux (kW/m^2)
St = Stanton number $= \frac{q''}{GC_p\Delta T_{sub}}$
T = temperature (K)
ΔT_{sub} = subcooled temperature difference (K)
V = coolant velocity (m/s)
ΔP = pressure drop (Pa)
η_{sub} = subcooling correction factor for the S&Z correlation

Subscripts

avg = average across and along the test section
b = bulk coolant
dem = demand side
fe = at the flow excursion point
ex = exit
ext = external
in = inside
s = saturated
sub = subcooling
ts = test section
w = wall

REFERENCES

1. M. Siman-Tov, et al., Thermal-Hydraulic Correlations for the Advanced Neutron Source Reactor Fuel Element Design and Analysis, *Proceedings of the ASME HTD Winter Annual Meeting*, American Society of Mechanical Engineers, Washington, December 1991.
2. M. Leddineg, Instability of Flow during Natural and Forced Circulation, *die Warme*, **61**(48): 891 898, 1938.

3. J. S. Maulbetsch and P. Griffith, A Study of System-Induced Instabilities in Forced-Convection Flows with Subcooled Boiling, Report No. 5382-35, *Department of Mechanical Engineering Massachusetts Institute of Technology*, Cambridge, Massachusetts, 1965.
4. E. D. Waters, *Heat Transfer Experiments for Advanced Test Reactor*, BNWL-216, UC-80 (TID-4500), 1966.
5. R. D. Boyd, Subcooled Water Flow Boiling Experiments under Uniform High Flux Conditions, *Fusion Tech.*, 13: 131 142, January 1988.
6. D. K. Felde et al., *Advanced Neutron Source Reactor Thermal-Hydraulic Test Loop Facility Description*, ORNL/TM-12397, Martin Marietta Energy Systems, Inc., Oak Ridge National Laboratory, 1994.
7. M. Siman-Tov et al., Experimental Investigation of Thermal Limits in Parallel-Plate Configuration for the ANSR, *29th National Heat Transfer Conference*, AIChE 89, 86 97, Atlanta, 1993.
8. M. Siman-Tov et al., *FY 1993 Progress Report on the ANS Thermal-Hydraulic Test Loop Operation and Results*, ORNL/M-3789, Martin Marietta Energy Systems, Inc., Oak Ridge National Laboratory, 1994.
9. M. W. Croft, *Advanced Test Reactor Burnout Heat Transfer Test*, ATR-FE-102, Babcock & Wilcox, 1964.
10. J. Costa, *Measurement of the Momentum Pressure Drop and Study of the Appearance of Vapor and Change in the Void Fraction in Subcooled Boiling at Low Pressure*, ORNL/TR-90/21, Union Carbide Corporation, Oak Ridge National Laboratory, 1967.
11. R. H. Whittle and R. Forgan, A Correlation for the Minima in the Pressure Drop vs Flow-Rate Curves for Sub-Cooled Water Flowing in Narrow Heated Channels, *Nuclear Eng. & Design*, 6: 89 99, 1967.
12. W. R. Gambill and R. D. Bundy, Heat Transfer Studies of Water Flow in Thin Rectangular Channels, Part I: Heat Transfer, Burnout, and Friction for Water in Turbulent Forced Convection. *Nucl. Science and Eng.*, 18: 69 79, 1964.
13. P. Saha and N. Zuber, Point of Net Vapor Generation and Vapor Void Fraction in Subcooled Boiling, *Proc. of 5th Int. Heat Transfer Conf.*, IV, 175 179, 1974.
14. M. Siman-Tov et al., Experimental Study of Static Flow Instability in Subcooled Flow Boiling in Parallel Channels, *4th ASME/JSME Thermal Engineering Joint Conference*, 1995.

15. J. Lafay, G. Maisonnier, and F. Girard, *Compte rendu d'essais flux de redistribution de debitexpulsion et calefactiona basse pression et qux faibles bitesses en canal rectangulaire*, TT/65-17-B/JL-GM-FG, 1965.
16. J. Costa et al., *Flow Redistribution in Research Reactors*, ORNL/TR-90/13, Martin Marietta Energy Systems, Inc., Oak Ridge National Laboratory, 1967.
17. M. Courtaud et al., *Compte rendu d'essais, boucle casimir Trace de courbes en S (Canal de 900 MM) Essais de depressurization*, TT/66-7-B/MC-GC-FM, March 1966.
18. M. Courtaud et al., *Compte rendu d'essais, boucle casimir Trace de courbes en S lere partie Eau degazee*, TT/66-2-B/MC-GC/FM, January 1966.
19. M. Courtaud et al., *Compte rendu d'essais Pertes de charge de redistribution de debit sur des canaux rectangulaires de 1.8 mm d'entrefer (Type R.H.F.)*, TT/67-7-B/MC-IS-GC-FM, June 1967.
20. P. Vernier, *Compte rendu d'essais Osirisetude de surete determination experimentale de courbes en s et des conditions de redistribution de debit*, TT/65-19-B/PV, 1965.
21. M. Courtaud et al., *Compte rendu d'essais, boucle casimir Trace de courbes en S sur des canaux a flux non uniforme*, TT/66-14-B/MC-GC-FM. June 1966.
22. K. Schleisiek and J. C. Dumaine, *Compte rendu d'essais Essais preliminaires pour RHF Determination experimentale des conditions de redistribution de debit aux pressions entre 4 et 5 kg/cm^2 abs pur un canal rectangulaire de 2 mm d'epaisseur et de 60 cm de longueur*, TT/66-10-B/KS/JCD, 27, 1966.
23. J. Lafay et al., *Compte rendu d'essais Influence de la repartition axiale du flux sur les seuils d'apparition de la redistribution de debit*, TT/68-4-B/JL, 1968.
24. H. Y. Cheh and C. F. Fighetti, *Flow Excursion Experimental Program Single Tube Uniformly Heated Tests*, CU-HTRF-T4, 1990.
25. R. Martin, Measurement of the Local Void Fraction at High-Pressure in a Heating Channel, *Nuclear Science and Engineering*, **48**, 125 138, 1972.
26. S. Z. Rouhani, Void Measurement in the Region of Subcooled and Low Quality Boiling, *Symposium on Two-Phase Flow*, University of Exeter, 1965.
27. R. Evangelisti and P. Lupoli, The Void Fraction in an Annular Channel at Atmospheric Pressure, *Int. J. Heat Mass Transfer*, **12**, 699 711, 1969.

28. G. W. Maurer, *A Method of Predicting Steady-State Boiling Vapor Fractions in Reactor Coolant Channels*, WAPD-BT-19, 1960.
29. R. A. Egen et al., *Vapor Formation and Behavior in Boiling Heat Transfer*, BMI 1163, 1957.
30. J. K. Ferrel, *A Study of Convection Boiling Inside Channels*, Ph.D. Thesis, Department of Chemical Engineering, North Carolina State University, Raleigh, North Carolina, 1964.
31. P. Griffith et al., Void Volumes in Sub-cooled Boiling, *ASME Paper 58HT-19*, U.S. National Heat Transfer Conference, Chicago, 1958.
32. F. W. Staub et al., *Heat Transfer and Hydraulics the Effects of Subcooled Voids*, NYO-3679-8, May 1969.
33. Z. Edelman and E. Elias, Void Fraction Distribution in Low Flow Rate Subcooled Boiling, *Nuclear Engineering and Design*, **66**, 375 382, February 1981.
34. J. T. Rogers et al., The Onset of Significant Void in Up-Flow Boiling of Water at Low Pressure and Velocities, *Int. J. Heat Mass Transfer*, **30**(11) 2247 2260, 1987.
35. G. G. Bartolemei et al., An Experimental Investigation of True Volumetric Vapour Content with Subcooled Boiling in Tubes, *Thermal Engineering*, **29**(3) 20 22, 1982.
36. E. L. Bibeau and M. Salcudeau, The Effect of Flow Direction on Void Growth at Low Velocities and Low Puressre, *Int. Comm. Heat Mass Transfer*, **17**, 19 25, 1990.
37. D. A. Labuntsov et al., The Main Principles of Variation in Vapour Content of Equilibrium and Non-equilibrium Two-phase Flows in Channels of Different Geometry, *Teploenergetika*, **31**, (9), 45 47, 1984.
38. K. Chen and J. F. King, *FlowTran Benchmarking with Onset of Flow Instability Data from 1963 Columbia University Experiment*, DPST-88-666, DE92 016492, October 1988.
39. G. G. Bartolemei and V. M. Chanturiya, Experimental Study of the True Void Fraction When Boiling Subcooled Water in Vertical Tubes, *Teploenergetika*, **14**(2) 80 83, 1967.

Fig. 1. Cross-section of the test channel in the thermal-hydraulic test loop.

Fig. 2. Nondestructive flow excursion data from the thermal-hydraulic test loop.

Fig. 3. Destructive flow excursion and critical heat flux data from the thermal-hydraulic test loop.

Fig. 4. Comparison between the modified and unmodified forms of the Saha and Zuber correlation for the Stanton number.

Fig. 5. Comparison between the modified and unmodified forms of the Saha and Zuber correlation for the Nusselt number.

Table 1. Flow excursion and critical heat flux data from the thermal-hydraulic test loop.[a,b]

TS #	Test Case	q''_{avg} (MW/m²)	q''_{ex} (MW/m²)	V_{ex} (m/s)	ΔP_{in} (MPa)	P_{ex} (MPa)	$T_{b,ex}$ (°C)	$\Delta T_{sub,ex}$ (°C)	Heat Loss %	Pe	Nu	St
3/C	FEN17B	7.6	7.9	014.4	0.296	1.721	182.5	22.7	7.6	205,876	1,269	0.0062
3/C	FEN17C	10.6	11.3	020.0	0.508	1.693	178.1	26.4	6.4	284,838	1,562	0.0055
3/C	FEN20A	12.0	13.6	021.9	0.604	1.725	178.6	26.9	6.3	311,628	1,835	0.0059
3/C	FEN20B	13.7	16.0	023.5	0.742	1.712	180.0	25.2	4.8	335,767	2,320	0.0069
3/C	FEN30A	13.6	15.8	023.6	0.754	1.709	180.7	24.4	4.6	336,222	2,364	0.0070
3/C	FED15B	11.6	13.0	019.7	0.545	1.706	181.9	23.0	5.5	280,980	2,064	0.0073
3/C	FED15C	13.0	14.7	021.4	0.632	1.719	181.3	24.1	5.1	305,312	2,238	0.0073
3/C	FED17A	14.4	16.1	023.5	0.747	1.685	176.8	27.7	6.1	335,044	2,117	0.0063
3/C	FED28B	14.6	15.5	023.0	0.765	1.723	181.1	24.4	5.5	328,534	2,316	0.0071
3/C	FE105B	9.0	9.9	015.4	0.359	1.721	173.6	31.6	6.2	218,953	1,142	0.0052
3/C	FE105C	12.7	14.3	020.1	0.657	1.722	179.1	26.3	4.9	286,543	1,986	0.0069
3/C	FE105D	14.8	16.3	023.1	0.919	1.707	182.5	22.6	4.4	329,534	2,645	0.0080
3/D	FE114B	10.8	11.8	020.1	0.567	1.713	181.9	23.2	4.8	284,618	1,840	0.0065
3/D	CF115B	11.8	13.0	019.8	0.628	1.709	186.1	18.9	4.2	279,712	2,497	0.0089
3/D	CF115B[c]	11.8	13.0	014.5	1.262	1.860	209.2	-0.5	4.5	209,575	—	—
3/E	FE210B	11.4	13.9	020.1	0.618	1.718	178.2	27.1	5.9	287,451	1,882	0.0065
3/E	FE212A	12.1	13.3	019.3	0.653	1.708	185.2	19.7	5.6	277,212	2,484	0.0090
3/E	FE212A[c]	12.1	13.0	017.8	0.785	1.738	194.8	10.6	7.4	255,764	4,519	0.0177
3/F	FE318B	1.9	2.2	005.0	0.078	0.445	132.7	15.1	12.4	69,035	511	0.0074
3/F	FE318B[c]	2.1	2.3	004.5	0.106	0.451	142.2	6.0	16.4	62,436	1,360	0.0218
3/G	FE330A	12.0	14.0	021.1	0.577	1.709	174.7	30.3	3.6	302,334	1,686	0.0056
3/G	FE331A	12.0	13.7	019.6	0.549	1.698	178.4	26.3	8.8	279,854	1,906	0.0068
3/G	FE331A[c]	11.5	12.4	018.3	0.634	1.708	181.8	22.8	9.6	261,321	1,997	0.0076
3/J	FE712B	1.7	1.9	002.9	0.033	1.695	183.1	21.1	12.2	41,606	332	0.0080
3/J	FE713B	0.7	0.7	002.8	0.025	0.175	100.1	16.2	15.1	41,659	159	0.0038
3/J	FE714B	4.3	5.0	008.6	0.142	1.700	174.3	30.2	6.5	122,923	604	0.0049
3/J	FE714C	6.4	7.2	011.6	0.248	1.701	182.3	22.2	5.5	166,044	1,199	0.0072
3/J	FE715B	9.2	10.8	016.6	0.440	1.709	177.0	27.9	3.1	237,797	1,424	0.0060
3/J	FE719B	11.7	14.8	020.1	0.634	1.673	176.8	27.1	3.8	288,280	1,999	0.0069
3/K	FE324C	5.6	6.5	009.4	0.137	1.726	182.8	22.0	7.7	135,764	1,086	0.0080
3/K	CF328A	12.3	13.8	019.3	0.592	1.715	181.2	23.6	6.7	278,253	2,170	0.0078
3/K	CF328A[c]	10.5	11.0	014.0	1.098	1.850	208.8	-0.3	6.2	206,178	—	—
3/L	FE511B	14.7	15.5	025.0	1.074	1.700	185.8	20.3	5.2	362,032	2,830	0.0078
3/L	FE511C	16.8	17.9	028.4	1.432	1.680	184.3	21.6	5.2	411,128	3,074	0.0075
4/A	FE620B	4.3	4.6	006.3	0.026	1.723	188.7	16.3	5.0	104,931	1,212	0.0116
4/A	CF622B	6.5	7.1	009.7	0.103	1.726	185.9	19.2	4.2	160,536	1,561	0.0097
4/A	CF622B[c]	5.7	4.7	004.7	0.353	1.997	212.4	0.0	11.0	80,146	—	—

[a] In all cases the inlet temperature is nominally 45 °C, except for FE318B where the inlet temperature is 40°C.

[b] Most flow excursion tests are nondestructive with data shown for the minimum pressure drop point.

[c] Refers to a true destructive burnout with FE and CF indicating FB and CHF tests, respectively.

[d] The channel gap for cases FE620B and CF622B was uncertain and had to be adjusted.

Table 2. Summary of the flow excursion/onset of significant voiding database used in present analysis[a]

Author	Data Points	Velocity (m/s)	Pressure (MPa)	Heat Flux (MW/m²)	ΔT_{sub} (°C)
THTL	31	2.6 - 25.3	0.18 - 1.74	0.7 - 20.1	15.1 - 31.6
Lafay et al (1965)	34	0.5 - 4.5	0.17	0.3 - 2.4	2.1 - 25.0
Lafay (1965) & Costa et al. (1967)	117	2.2 - 7.7	0.17 - 0.39	0.7 - 4.6	2.3 - 42.1
Courtaud et al (March 1966)	6	2.5 - 9.0	0.3	2.0 - 4.0	11.3 - 22.2
Courtaud et al (Jan. 1966)	15	1.8 - 7.0	0.28 - 0.32	2.0 - 4.0	11.8 - 24.7
Courtaud et al (June 1967)	12	4.8 - 8.8	0.29 - 1.08	4.0 - 7.0	11.0 - 22.4
Vernier (1965)	19	2.1 - 10	0.15 - 0.29	1.0 - 4.5	6.6 - 16.5
Courtaud et al (June 1966)	12	2.0 - 6.2	0.3	2.0 - 4.0	17.6 - 47.2
Whittle & Forgan (1967)	23	1.6 - 4.5	0.10 - 0.12	0.7 - 2.1	3.7 - 9.7
Whittle & Forgan (1967)	65	0.8 - 11.4	0.12 - 0.17	0.4 - 3.5	4.6 - 16.3
Schleisiek & Dumaine (1966)	14	3.6 - 9.0	0.39 - 0.49	2.5 - 5.1	11.2 - 18.8
Lafay, et al (1968)	18	1.6 - 9.2	0.49	2.0 - 6.0	5.4 - 33.6
Waters (1966)	17	0.5 - 17.8	0.27 - 2.52	0.1 - 10.1	6.0 - 24.6
Chen & Fighetti, et al (1990)	81	1.3 - 7.9	0.24 - 0.46	1.1 - 3.2	2.2 - 43.7
Croft (1964)	30	7.9 - 18.1	0.57 - 1.74	3.0 - 12.2	4.7 - 29.3
Martin (1972)	15	0.7 - 4.8	7.85 - 13.73	0.2 - 1.7	1.6 - 12.0
Maulbetsch & Griffith (1965)	47	2.0 - 18.1	0.21 - 0.41	3.2 - 12.6	21.1 - 65.4
Rouhani (1966) AE	12	0.1 - 1.5	0.98 - 5.00	0.3 - 0.9	7.2 - 20.0
Evangelisti & Lupoli (1969)	3	0.6 - 1.5	0.11	0.4 - 0.9	12.7 - 21.5
Maurer (1960)	15	0.7 - 6.9	8.27 - 13.79	0.3 - 3.8	3.7 - 31.7
Egen et al (1957)	7	0.8 - 1.7	13.79	0.3 - 1.6	4.4 - 21.1
Ferrell (1964)	11	0.6 - 1.4	0.41 - 1.66	0.2 - 0.7	10.6 - 18.9
Costa (1967)	43	2.4 - 8.0	0.17 - 0.50	1.0 - 4.2	9.5 - 32.5
Griffith et al (1958), BETHS	12	0.8 - 1.7	8.27 - 13.79	0.3 - 1.9	6.1 - 41.7
Rouhani (1965), BMI	11	0.2 - 1.6	0.98 - 5.00	0.3 - 0.9	11.1 - 32.2
Staub et al (1969), Task I	28	0.2 - 3.0	0.09 - 0.3	0.2 - 0.8	3.3 - 13.7
Staub et al (1969), Task III	18	0.9 - 3.4	0.73 - 10.37	0.4 - 1.7	9.1 - 28.6
Edelman & Elias (1981)	16	0.03 - 0.2	0.10	0.01 - 0.1	0.6 - 3.9
Rogers et al (1987)	16	0.1 - 0.5	0.16	0.3 - 1.2	7.9 - 25.9
Bartolemei et al (1982)	17	0.4 - 3.1	3.01 - 14.75	0.4 - 2.0	7.4 - 54.4
Bibeau & Salcudean (1990)	10	0.2 - 0.5	0.16	0.3 - 1.0	9.5 - 54.9
Labuntsov, et al (1984)	6	1.0 - 4.0	2.00 - 7.00	0.6 - 1.2	8.6 - 15.4
Chen & King (1988)	5	6.9 - 9.8	0.19	2.0 - 3.0	0.1 - 5.2
Bartolemei & Chanturiya (1967)	16	1.0 - 1.1	1.50 - 4.50	0.4 - 0.8	9.7 - 30.8
Total	802	0.03 - 25.3	0.1 - 14.75	0.01 - 20.1	0.1 - 65.4

[a] Complete citations are located in the references.

[b] (St) number was independently calculated from reports data.

Table 3. U factor[a] statistics for Costa, S & Z, and Modified S & Z correlations.[c]

Peclet Range	Correlation	Data Range	# Points	Average	S.D.[(b)]	S.D.%
Pe > 70,000 *(Stanton Correlation)*	Costa	*THTL Data*	28	1.50	0.35	23.4
		All Data	634	1.38	5.10	369.5
		V > 8 m/s	105	3.07	12.34	401.9
		V < 8 m/s	529	1.04	0.68	65.2
	Saha & Zuber	*THTL Data*	28	1.07	0.24	22.4
		All Data	634	1.54	3.48	226.4
		V > 8 m/s	105	2.22	8.40	377.7
		V < 8 m/s	529	1.40	0.75	53.1
	Modified Saha & Zuber	*THTL Data*	28	1.03	0.16	15.9
		All Data	634	1.02	0.30	29.7
		V > 8 m/s	105	1.10	0.20	18.5
		V < 8 m/s	529	1.00	0.31	31.5
Pe < 70,000 *(Nusselt Correlation)*	Saha & Zuber	*THTL Data*	3	0.75	0.41	54.9
		All Data	168	1.28	0.85	66.4
	Modified Saha & Zuber	*THTL Data*	3	0.62	0.31	50.9
		All Data	168	0.84	0.55	66.0

[a] U = Experimental Heat Flux / Predicted Heat Flux

[b] S.D. = One Standard Deviation of U.

[c] Includes a data point with a subcooling of 0.14°C.

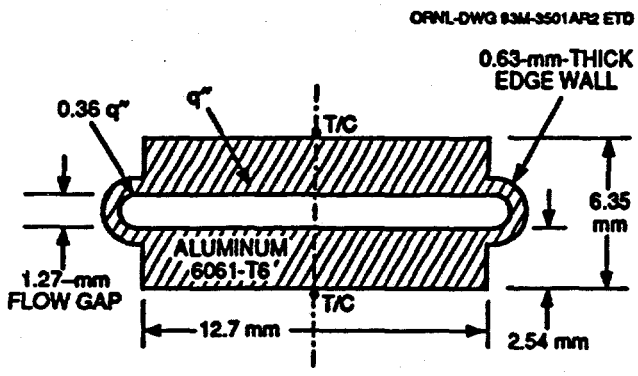

Fig. 1. Cross-section of the test channel in the thermal hydraulic test loop.

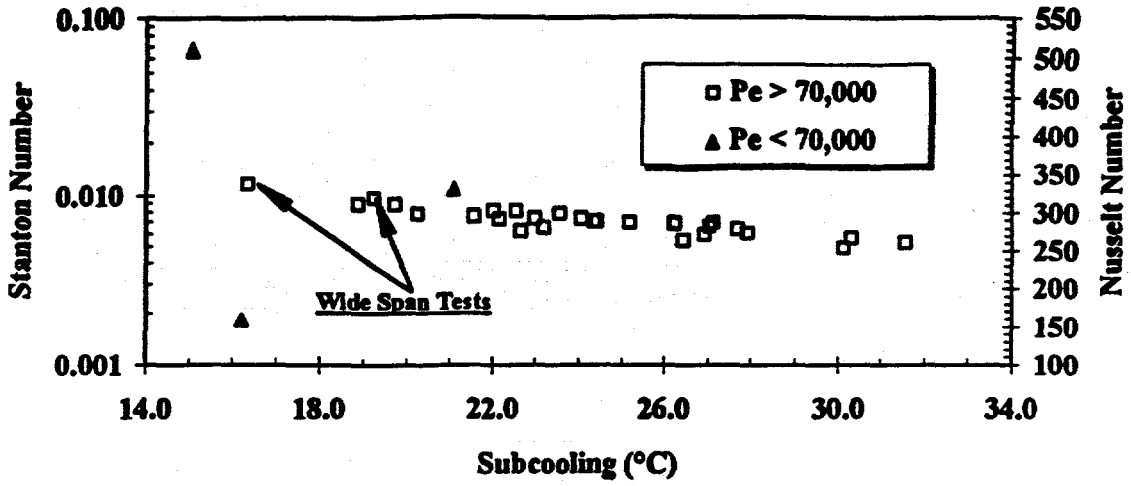

FIGURE 2. NON-DESTRUCTIVE FLOW EXCURSION DATA FROM THE THERMAL HYDRAULIC TEST LOOP.

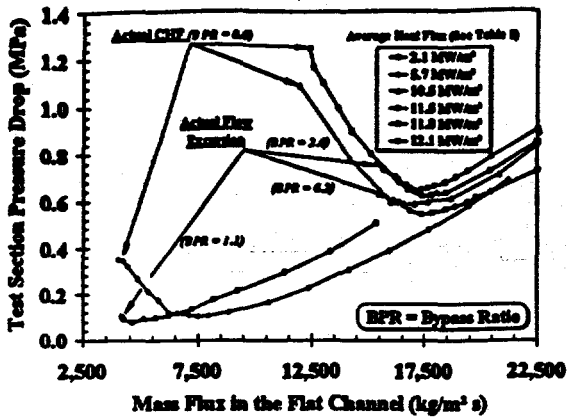

Figure 3. DESTRUCTIVE FLOW EXCURSION AND CRITICAL HEAT FLUX DATA FROM THE THERMAL HYDRAULIC TEST LOOP.

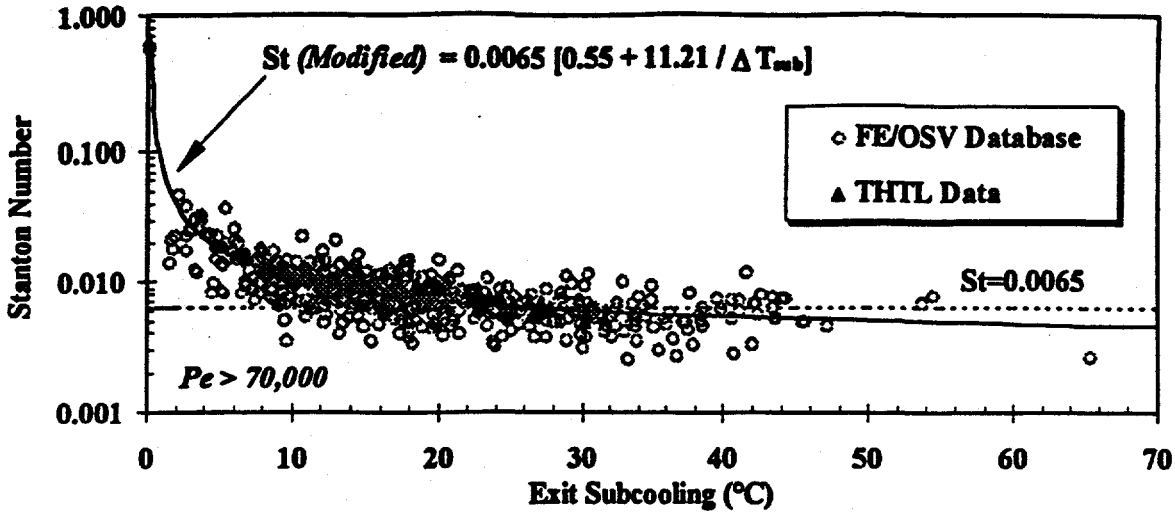

Figure 4. COMPARISON BETWEEN THE MODIFIED AND UNMODIFIED FORMS OF THE SAHA ZUBER CORRELATION *FOR St NUMBER.*

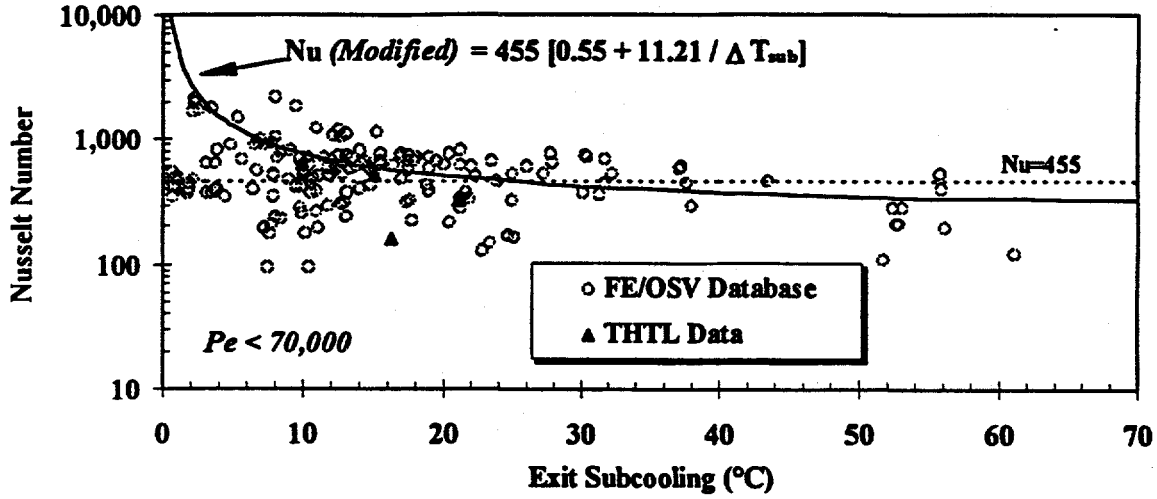

Figure 5. COMPARISON BETWEEN THE MODIFIED AND UNMODIFIED FORMS OF THE SAHA ZUBER CORRELATION *FOR Nu NUMBER.*